A remote sensing approach for estimating distributed daily net carbon dioxide flux in semiarid grasslands

C. D. Holifield Collins,[1] W. E. Emmerich,[1] M. S. Moran,[1] M. Hernandez,[1] R. L. Scott,[1] R. B. Bryant,[1] D. M. King,[2] and C. L. Verdugo[1]

Received 1 November 2006; revised 18 January 2008; accepted 18 April 2008; published 20 May 2008.

[1] Semiarid systems compose a significant portion of the world's terrestrial area and may play an important role in the global carbon cycle. A model was developed using the relation between surface reflectance and temperature obtained from satellite imagery to determine a Water Deficit Index (WDI) that estimated distributed plant transpiration, and by extension carbon dioxide (CO_2) flux, for a point in time. Relationships were developed to scale these instantaneous flux measurements up to daytime estimates, which were then used to obtain measures of nighttime flux. Satellite images were acquired for a 5-year period (1996–2000) during which transpiration and net CO_2 flux were measured for a semiarid grassland site in southeastern Arizona. Manual and automatic chamber data were also collected at the same site during the monsoon growing seasons of 2005 and 2006 and used to develop the relationship between and daytime and nighttime CO_2 flux. Strong linear relationships were found between WDI-derived instantaneous and daytime net CO_2 flux estimates ($R^2 = 0.97$), and between daytime and nighttime fluxes ($R^2 = 0.88$). These relations were used to generate maps of distributed total daily net CO_2 flux. The error for the model was within the range of error inherent in the data sets used to create it and remained reasonable when used with WDI values less than 0.9. This study demonstrated that remote sensing can offer a physically based means of obtaining daily net CO_2 flux in semiarid grasslands.

Citation: Holifield Collins, C. D., W. E. Emmerich, M. S. Moran, M. Hernandez, R. L. Scott, R. B. Bryant, D. M. King, and C. L. Verdugo (2008), A remote sensing approach for estimating distributed daily net carbon dioxide flux in semiarid grasslands, *Water Resour. Res.*, *44*, W05S17, doi:10.1029/2006WR005699.

1. Introduction

[2] The global concentration of carbon dioxide (CO_2) in the atmosphere is increasing, largely as a result of human activities such as burning fossil fuels and biomass as fuel [*Intergovernmental Panel on Climate Change*, 2005]. Efforts to alleviate global climate change through the increased use of sequestration have resulted in a continuing search for more accurate quantification of global terrestrial carbon sources and sinks [*Bachelet et al.*, 2001]. A large portion of this research has been focused on forest and temperate grassland ecosystems [*Xiao et al.*, 2004; *Dugas et al.*, 1999; *Gilmanov et al.*, 2005; *Frank and Dugas*, 2001; *Novick et al.*, 2004; *Baldocchi and Wilson*, 2001; *Wilson and Baldocchi*, 2001; *Valentini et al.*, 2000; *Baldocchi et al.*, 2001]. However, the role that semiarid areas may play in this quantification has not been studied as extensively. Approximately 15% of the world's terrestrial area is classified as semiarid, the majority of which is covered by grasslands [*Niemeijer et al.*, 2005]. Because of findings that semiarid systems may serve as CO_2 sinks as well as sources [*Emmerich*, 2003], further study of these systems is needed.

[3] The most common means of measuring and monitoring daily net CO_2 fluxes is through the use of eddy covariance (EC) and Bowen ratio energy balance (BREB) instrumentation [*Baldocchi et al.*, 2001; *Svejcar et al.*, 1997]. These systems are micrometeorological approaches for estimating CO_2 and water fluxes at specific sites. The eddy covariance technique is a direct method of measuring fluxes while the BREB technique measures fluxes indirectly [*Wylie et al.*, 2003]. Both methods have their advantages and disadvantages, but both have been shown to be appropriate methods for obtaining CO_2 flux measurements [*Dugas*, 1993; *Baldocchi et al.*, 2001] at the local scale. Extensive networks of EC and BREB systems have been set up throughout the world to measure CO_2 [*Baldocchi et al.*, 2001; *Svejcar et al.*, 1997]. These networks have been a great source of basic information about net CO_2 flux, because the instrumentation can be maintained at one location for temporally continuous measurements over a season or over several years. However, the measurements are limited to a small area defined by the fetch of the instrumentation. Furthermore, owing to less reliable energy balance, concentration gradients, and wind speeds needed for calculations, these systems are more suited for daytime rather than nighttime use [*Franzluebbers et al.*, 2002].

[1] Southwest Watershed Research Center, Agricultural Research Service, U.S. Department of Agriculture, Tucson, Arizona, USA.
[2] School of Natural Resources, University of Arizona, Tucson, Arizona, USA.

0043-1397/08/2006WR005699$09.00

[4] Similarly, manual and automatic chambers are methods commonly used to obtain measurements of soil CO_2 flux, or soil respiration. The manual chamber method offers the advantage of providing spatial measurements of an area of interest, as several measurement collars can be installed throughout the measurement area. However, owing to time constraints of the operators, temporally continuous measurements cannot easily be obtained. Automated chambers eliminate this problem of limited temporal frequency, but introduce a limitation in spatial coverage. Because these systems are often more expensive and require greater infrastructure for operation, installing the number of chambers needed to capture spatial variability is commonly not feasible [*Savage and Davidson*, 2003]. Nevertheless, these chamber-based methods are useful for measuring both daytime and nighttime soil respiration [*Dugas*, 1993; *Franzluebbers et al.*, 2002; *Huxman et al.*, 2004; *Buchmann*, 2000; *Davidson et al.*, 2002; *Potts et al.*, 2006].

[5] Chambers and micrometeorological instrumentation are both limited to point-based measurements and, even with a network of sensors, have not been able to capture regional spatial variability. It is recognized that measurements with greater spatial coverage are needed to quantify regional net CO_2 flux and to examine the role semiarid systems play in the continental and global carbon cycles.

[6] Remote sensing has the capability to provide instantaneous, large-scale spatial measurements of terrestrial surfaces. Work has already been conducted to use remote sensing to model CO_2 flux at the regional [*Wylie et al.*, 2003, 2004; *Lim et al.*, 2004; *Gilmanov et al.*, 2005] and global scales [*Box et al.*, 1989; *Prince and Goward*, 1995; *Lafont et al.*, 2002]. These studies have typically used a combination of the Normalized Difference Vegetation Index (NDVI), a measure of vegetation greenness, derived from coarse resolution (1 or 4 km) satellite imagery (e.g., Advanced Very High Resolution Radiometer (AVHRR); SPOT-4 VEGETATION) and EC, BREB, or modeled data measurements as the basis for their estimates. Many of these studies found strong relationships between NDVI and gross primary production (GPP) or biomass, but found that the relationships became weaker when only NDVI was used to try and obtain daily CO_2 flux. This was partly from the lack of a strong relationship between NDVI and nighttime respiration, but more importantly from the biases that can occur when vegetation is undergoing stress that affects photosynthetic process but not greenness.

[7] The Water Deficit Index (WDI) is a technique based on a vegetation index-temperature (VIT) trapezoid that combines a spectral vegetation index and surface temperature to estimate evapotranspiration for full-cover and partially vegetated sites [*Moran et al.*, 1994], and has been previously been used to evaluate water stress in agricultural fields for irrigation scheduling [*Moran et al.*, 1994; *Moran*, 1994; *Colaizzi et al.*, 2003], drought monitoring [*ShuaHua et al.*, 2005], and even fire prediction [*Vidal and Devaux-Ros*, 1995]. By capitalizing on the link that exists between plant transpiration and net CO_2 plant uptake or net primary production (NPP), rather than vegetation greenness like the previously mentioned studies, the WDI also has the potential to estimate net CO_2 flux in actively transpiring vegetation.

[8] *Moran et al.* [1996] demonstrated that the WDI could be used to obtain reasonable estimates of evapotranspiration in semiarid grasslands, as well as several other semiarid biomes. Further, *Holifield et al.* [2003] has shown that the WDI can be used in combination with Landsat satellite imagery to obtain instantaneous spatially distributed estimates of transpiration in semiarid grasslands. Thus, it may be possible to obtain estimates of instantaneous net CO_2 flux which can be extrapolated up to a daytime (12-h) temporal scale using remote sensing. However, this would only tell half of the story. Nighttime net CO_2 flux, dominated by soil respiration, comprises a significant portion of total daily net CO_2 flux and cannot be ignored [*Wohlfahrt et al.*, 2005]. *Box et al.* [1989] stated that respiration appeared to be almost linearly increased with increasing amounts of live standing biomass, implying a possible connection between daytime and nighttime net CO_2 flux. The existence of such a relationship would provide a means of inferring nighttime net CO_2 flux from satellite derived daytime net CO_2 flux, making it possible to obtain daily net CO_2 flux at the landscape scale through remote sensing. This idea of utilizing remote sensing to obtain daily net CO_2 flux at the landscape scale was the focus of this study, and was explored though a series of objectives. The objectives were to: (1) derive instantaneous CO_2 flux for a semiarid Chihuahuan Desert grassland site using the WDI; (2) estimate net daytime CO_2 flux from the WDI-derived instantaneous estimate; (3) derive the relation between daytime and nighttime net CO_2 flux; and (4) generate maps depicting spatially distributed estimates of total daily net CO_2 flux in a semiarid grassland.

2. Methods and Data Processing

[9] This study was conducted within the USDA Agricultural Research Service, Southwest Watershed Research Center, Walnut Gulch Experimental Watershed (WGEW). Landsat scenes acquired over 9 years (1990, 1992–1995, and 1997–2000) during the monsoon season were used, along with 10 years (1996–2000, 2002–2006) of Bowen ratio energy balance measurements, 4 years (2002–2005) of ground reflectance and surface temperature measurements, 2 years (2005–2006) of data from an automated chamber, 1 year (2005) of data from a manual chamber, and coincident meteorological measurements.

2.1. Study Area and Instrumentation

[10] The WGEW, located in the San Pedro Valley of southeast Arizona encompasses the city of Tombstone, covers 150 km^2 and is representative of approximately 60 million hectares of the brush and grass-covered rangeland found throughout the semiarid southwestern United States [*Renard et al.*, 1993]. The Chihuahuan desert grassland area examined for this study was approximately nine square kilometers in size and located within the upper portion of the watershed (Figure 1), which is dominated by black grama (*Bouteloua eriopoda*), blue grama (*B. gracilis*), sideoats grama (*B. curtipendula*), bush muhly (*Muhlenbergia porteri*), and Lehmann lovegrass (*Eragrostis lehmanniana*).

[11] A Bowen ratio energy balance system (BREB) (Model 023/CO_2 Campbell Scientific Inc., Logan, UT, USA) was located within the study area. The system has a fetch of >200 m in all directions and makes continuous 20 min average carbon and water vapor flux measurements. Atmospheric gradients of air temperature, moisture and CO_2

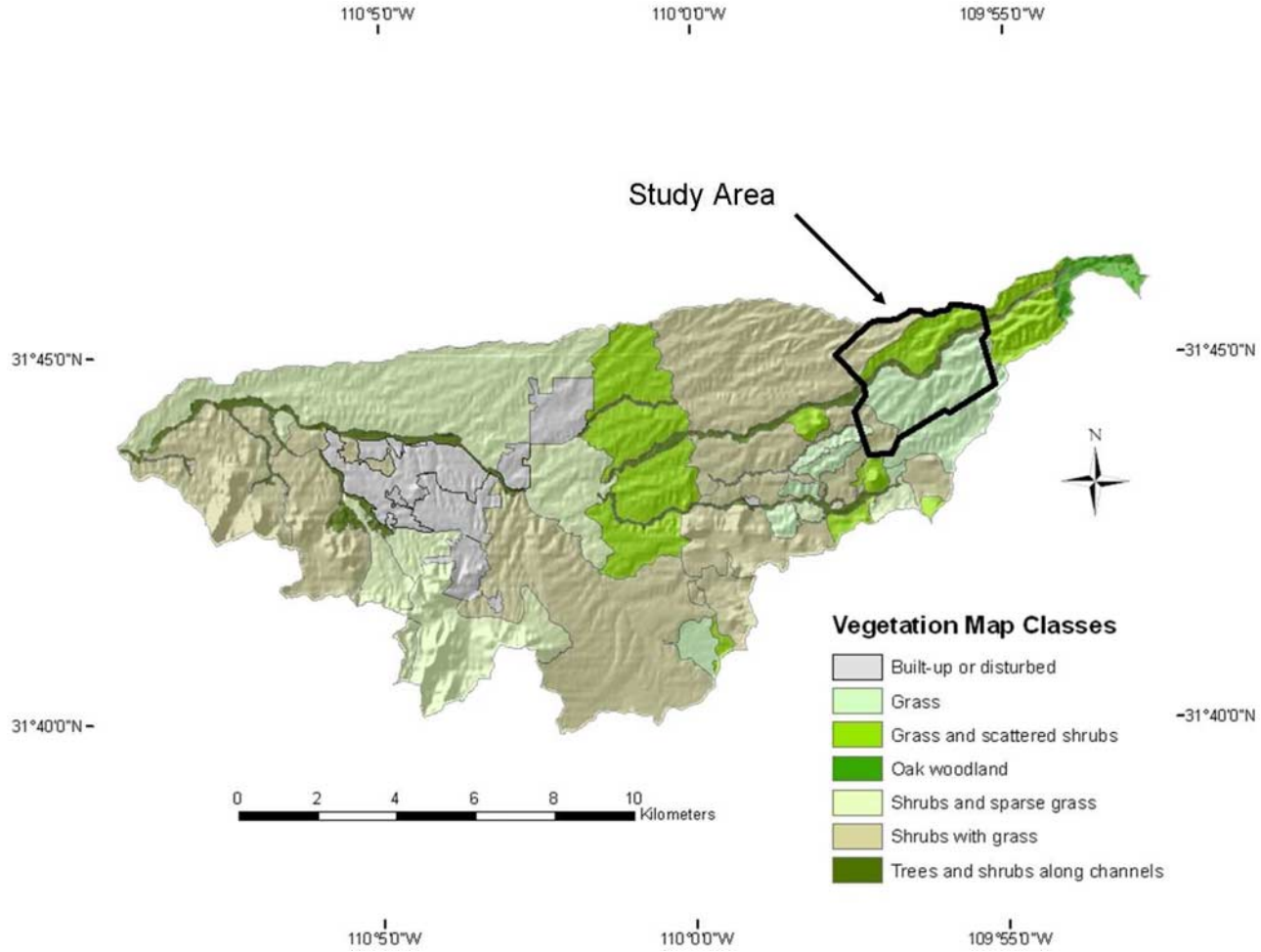

Figure 1. Vegetation map [*Skirvin et al.*, 2008] containing the 9 km^2 study area located within the Walnut Gulch Experimental Watershed.

were measured every 2 s and averaged every 20 min. The 20 min averages were stored in a data logger (model 21X, Campbell Scientific Inc). Atmospheric carbon dioxide and moisture concentrations were measured with an infrared gas analyzer (IRGA) (LI-6262, LI-COR Inc., Lincoln, NE, USA). A brief description of the meteorological data collection and of how the carbon and water vapor fluxes were calculated is presented by *Emmerich* [2003]. Detailed discussions of the theory and procedures used to calculate the carbon and water vapor fluxes are presented by *Dugas* [1993] and *Dugas et al.* [1999]. For this study, positive net flux indicates CO_2 entering the ecosystem, while negative net flux indicates a loss of CO_2.

2.2. Automated Chamber Measurements

[12] Automated soil respiration measurements were made every 30 min near an EC micrometeorological tower located within the study area. The chamber was a 0.25 m diameter ring set into the soil upon which an Acrylic dome was lowered every 30 min resulting in a chamber volume of 8.09 L. Once the lid was lowered, a small fan circulated the air within the chamber, and the CO_2 concentration of the air from the chamber was sampled in a closed loop by a gas analyzer (LI-840, Li-Cor Inc., Lincoln, NE) every 0.1 s for a total of four minutes or until the CO_2 concentration had risen to a maximum of 150 ppm, which ever came first. A regression line was fit to the CO_2 versus time plot from the time the chamber was completely closed to just before it opened to determine the flux rate. In 2005, the gas analyzer was manually calibrated approximately every two weeks. In 2006, the calibration was automated and the IRGA was calibrated daily. Calculated fluxes were discarded for regressions with $R^2 < 0.90$.

2.3. Collar Measurements Collected Using a Manual Chamber

2.3.1. Field Design

[13] A measurement plot 100 m × 100 m with four transects 100 m long was laid out for the manual collar measurements. The plot straddled a small northeast running ridge, with a small portion lying on the ridge top and the rest falling off onto north and south facing slopes. The 100 m transects were placed 20 m apart and the whole grid was centered at the BREB system located within the study area (Figure 2). A total of 20 collars were laid out within the measurement plot. Collars were made from thin-walled polyvinyl chloride (PVC) pipe with an interior diameter of 10 cm, and a 5 cm height with approximately 2.5 cm protruding when inserted into the ground. All collars were painted with brown paint similar to the soil color to avoid

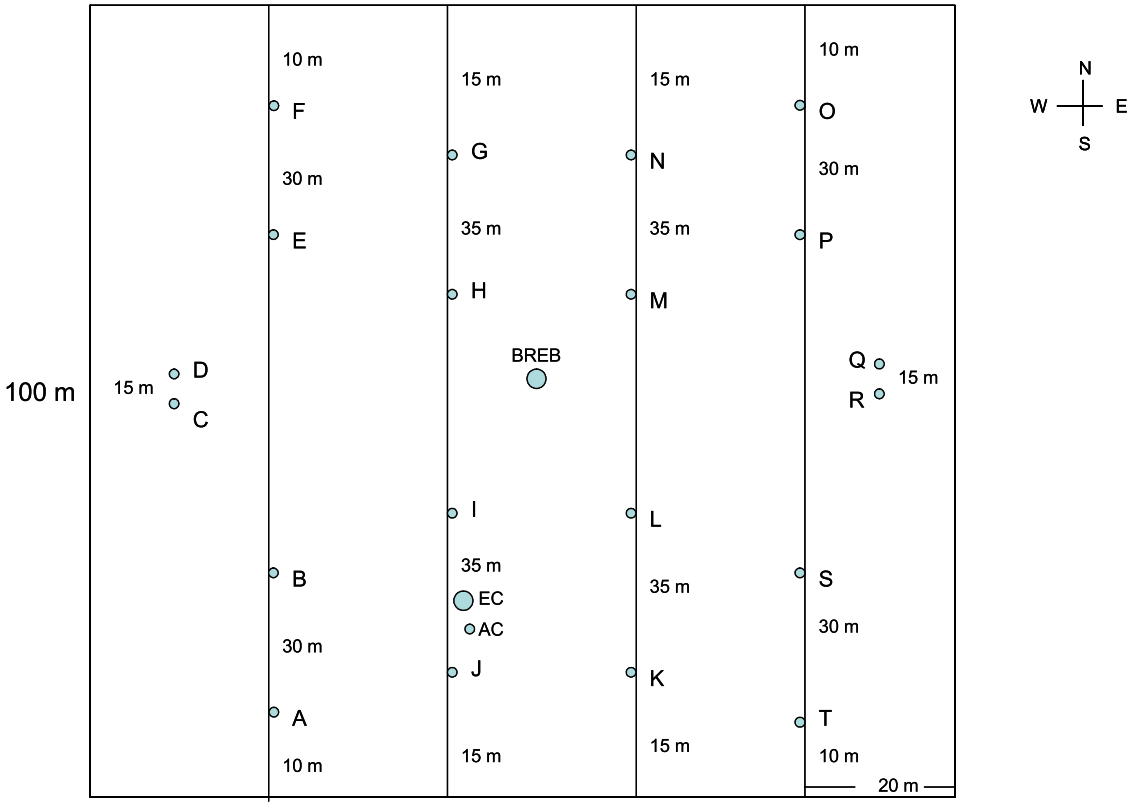

Figure 2. Map of field design centered on Bowen ratio energy balance (BREB) system. Letters A–T designate collar locations. Locations for the eddy covariance (EC) system and automated chamber (AC) are also indicated.

the artificial heating or cooling that can occur with white or black surfaces. The total number of collars was determined on the basis of time constraints related to performing the measurements. Measurement time per collar was approximately 5 min resulting in a total measurement time of two hours per measurement cycle.

[14] The collars were placed along the measurement grid according to the plot map shown in Figure 2. Sixteen collars were arranged over bare soil along the transect lines with four collars per transects. The distances marked between the collars (10 m, 15 m, 30 m, and 35 m) were the distances from the boundary of the 100 m x 100 m plot. The remaining four collars were placed as pairs 15 m in from the outside West and East plot boundaries. Each pair consisted of one collar over bare soil and the other over a small tuft of grass. These pairs were installed to provide an opportunity to perform comparisons between plant and soil respiration. For identification purposes, each collar was marked using a stake of metal rebar covered by PVC marked with reflective tape and a reflective letter. Plot corners were marked with rebar within PVC marked with double strips of reflective tape.

2.3.2. Description of Instrumentation and Measurement Protocol

[15] Soil respiration measurements were collected using a portable photosynthesis system (LI-6200 with an LI-6250 CO_2 infrared gas analyzer (IRGA), LI-COR Inc., Lincoln, NE, USA), fitted with a soil respiration chamber (LI-6000–09, LI-COR Inc., Lincoln, NE, USA). The head attached to the chamber top contained sensors for measuring soil temperature, chamber air temperature and humidity, and had tubing for entry and exit of circulating gas between the chamber and the IRGA in the photosynthesis system. The soil chamber volume was 9.6×10^{-4} m^3 and the surface area was 7.85×10^{-3} m^2.

[16] A vented, closed system was used to make the measurements. Therefore to eliminate leaks, CO_2 flux measurements were made below, at and above the ambient CO_2 concentration. Before beginning a measurement, the ambient CO_2 concentration at the soil surface was measured. After the chamber was placed onto the collar, the CO_2 scrubber was used to draw the CO_2 in the closed system down below the ambient concentration. The scrubber was turned off allowing CO_2 concentration to rise, and data were logged while the CO_2 concentration was below, at, and above the ambient level (LI-COR, 1993). Calibration was performed each day before measurements were taken using a small tank of CO_2 calibration gas with a known concentration of 500 ppm (Matheson Tri-Gas®). Collar measurements were made over 15 d (June–September) in 2005. Measurement cycles comprised three 2-hour periods (6:00 P.M. to 8:00 P.M.; 10:00 P.M. to 12:00 A.M.; 4:00 A.M. to 6:00 A.M.).

2.4. Image Processing

[17] Nine years (1990, 1992–1995, and 1997–2000) of Landsat-5 Thematic Mapper (TM) and Landsat-7 Enhanced Thematic Mapper Plus (ETM+) satellite images of the WGEW collected during the summer monsoon period (1 June–31 October) were used for this study (Tables 1a

Table 1a. Landsat Image Dates and Overpass Times for Scenes of the Walnut Gulch Experimental Watershed[a]

Satellite Type	Image Date	Overpass Time	Time Period of T_p Value	T_p Value for 13 August 1999, g m^{-2} s^{-1}
Landsat-5 TM	14 October1997 (DOY 287)	1024	1020	0.1590
	30 August 1998 (DOY 242)	1030	1040	0.1596
	1 October 1998 (DOY 274)	1030	1040	0.1596
Landsat-7 ETM+	12 September 2000 (DOY 256)	1056	1100	0.1684
	28 September 2000 (DOY 272)	1056	1100	0.1684

[a]Maximum transpiration values measured on 13 August 1999 (DOY 225) at times coincident with satellite overpasses were used as potential transpiration (T_p) for the study. Time period of T_p value is indicative of measurement collected over the previous 20 min (e.g., 1020 is averaged measurement covering the period from 1000 to 1020).

and 1b). All images were geocorrected to subpixel accuracy using the nearest neighbor resampling method. The Refined Empirical Line (REL) approach [*Moran et al.*, 2001], which uses two points of known reflectance to determine a digital number (DN)-reflectance relation for spectral bands, was used to convert DN to reflectance for the green, red, and NIR spectral bands of each image. These particular images were selected for use because no substantial precipitation had occurred the day of, two days before, or after the image was taken. This criteria was used to ensure the soil surface was dry at the time the images were taken, making evaporation (E) negligible, and that humidity levels would not interfere with atmospheric correction.

[18] Satellite-based surface temperatures (t_s) were retrieved from Landsat-5 TM DN using the equation

$$t_s = (K2/[\ln(K1/\text{slope}(DN) + \text{offset} + 1)]) - \text{Kelvin}, \quad (1)$$

where slope = 0.005632, offset = 0.1238, Kelvin = 273.15, K1 = 60.766 and K2 = 1260.56 according to the technique outlined by *Lansing and Barker* [1985].

[19] The equation

$$t_s = [(17.04/254)(DN - 1)]/1000, \quad (2)$$

provided by *Schott et al.* [2001], was used to convert Landsat-7 ETM+ DN to t_s. *Moran* [1990] reported that the difference between the surface temperature and the temperature measured above the atmosphere by a Landsat sensor was typically 2°C for typical clear sky conditions in Arizona. Therefore, the t_s values computed using equations (1) and (2) were increased by 2°C to account for atmospheric attenuation. It should be noted that the need and methods employed for atmospheric correction are often location specific. The atmospheric correction employed in this study is specific for Arizona. Utilization of this method in other locations should include use of atmospheric corrections that are appropriate for those locations. These images of surface reflectance and temperature, as well as meteorological data acquired at the time of the satellite imagery, were used to compute the WDI.

2.5. Water Deficit Index (WDI)

[20] The WDI is a method for estimating evapotranspiration (ET) over large-scale heterogeneous areas. The WDI is based on a Vegetation Index/Temperature (VIT) Trapezoid (Figure 3) which combines a spectral vegetation index with surface temperature (combination of soil and vegetation temperatures) to determine water deficit conditions. The Soil-Adjusted Vegetation Index (SAVI) was the spectral vegetation index used for this study. SAVI was calculated using the following equation,

$$\text{SAVI} = (\rho_{\text{NIR}} - \rho_{\text{red}})/(\rho_{\text{NIR}} + \rho_{\text{red}} + L)(1 + L), \quad (3)$$

where ρ_{NIR} and ρ_{red} are the near-IR and red reflectances, and L is assumed to be 0.5 for a variety of leaf area index (LAI) values [*Huete*, 1988]. The shape of the trapezoid is not fixed and varies on the basis of the inputs used to compute the vertices. The trapezoid depicted in Figure 3 was created from data for 30 August 1998 in the semiarid grassland area used for this study. At this location, the SAVI typically does not exceed 0.4 (the broken line shown in Figure 3). Therefore, owing to the nature of the vegetation found in the study area, all trapezoids were restricted to the SAVI range of 0.1 to 0.3. However, it should be noted that the WDI was derived from the Crop Water Stress Index (CWSI) [*Jackson et al.*, 1981] developed in croplands, so in theory a trapezoid could be extended up to a SAVI of 0.8 for full cover vegetation.

[21] The surface temperature minus air temperature ($t_s - t_a$) values for the four vertices of the VIT Trapezoid were defined by combining the Penman-Monteith equation [*Monteith*, 1973] with energy balance equations, as originally proposed by *Jackson et al.* [1981]. The subscript '*n*' of $(t_s - t_a)_n$ refers to a vertex in Figure 3. Vertex 1 of the trapezoid represents full-cover, well watered vegetation and $(t_s - t_a)_1$ is computed as

$$(t_s - t_a)_1 = [r_a(R_n - G)/C_v]\left[\gamma\left(1 + r_{cp}/r_a\right)/\left\{\Delta + \gamma\left(1 + r_{cp}/r_a\right)\right\}\right] - \left[\text{VPD}/\left\{\Delta + \gamma\left(1 + r_{cp}/r_a\right)\right\}\right], \quad (4)$$

where r_a is the aerodynamic resistance (s m^{-1}), R_n the net radiant heat flux density (W m^{-2}), **G** the soil heat flux

Table 1b. Landsat Image Dates of Scenes of WGEW Used to Produce Maps of Distributed Daytime, Nighttime, and Total Daily Net CO_2 Flux

Satellite Type	Image Date
Landsat-5 TM	11 October 1990 (DOY 284)
	1 October 1992 (DOY 275)
	17 September 1993 (DOY 260)
	10 October 1994 (DOY 295)
	6 August 1995 (DOY 218)
	23 September 1995 (DOY 266)
	9 October 1995 (DOY 282)
Landsat-7 ETM+	26 September 1999 (DOY 269)
	26 July 2000 (DOY 208)

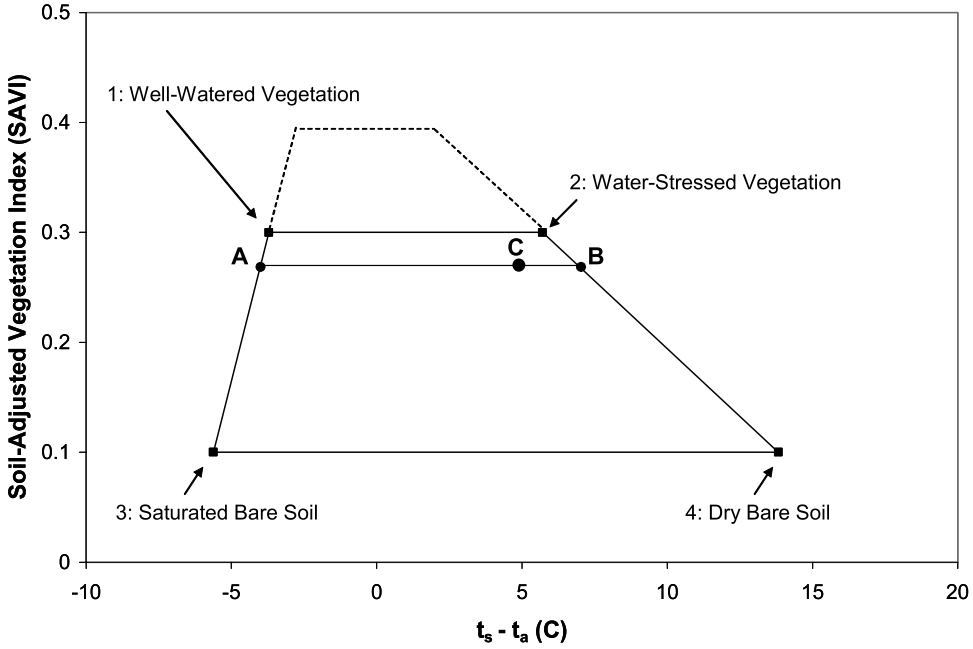

Figure 3. The Vegetation Index/Temperature Trapezoid for 30 August 1998 (DOY 242) within the semiarid grassland study area. The soil adjusted vegetation index (SAVI) ranges from ~0.1 for bare soil to ~0.3 for full-cover vegetation for this particular trapezoid. However, the SAVI range can be extended up to ~0.4 on the basis of the type of vegetation located within the study area (broken line). The water deficit index is equal to the ratio of AC/AB.

density (W m^{-2}), C_v the volumetric heat capacity of air (J $°C^{-1}$ m^{-3}), γ the psychometric constant (Pa $°C^{-1}$), r_{cp} the canopy resistance at potential evapotranspiration, Δ the slope of the saturated vapor pressure-temperature relation (Pa $°C^{-1}$), and VPD the vapor pressure deficit of the air (Pa). Vertex 2 represents full-cover vegetation with no available water and $(t_s - t_a)_2$ is computed as

$$(t_s - t_a)_2 = [r_a(R_n - G)/C_v][\gamma(1 + r_{cx}/r_a)/\{\Delta + \gamma(1 + r_{cx}/r_a)\}] - [VPD/\{\Delta + \gamma(1 + r_{cx}/r_a)\}], \quad (5)$$

where r_{cx} is the canopy resistance associated with nearly complete stomatal closure.Vertex 3 represents saturated bare soil and $(t_s - t_a)_3$ is computed as

$$(t_s - t_a)_3 = [r_a(R_n - G)/C_v][\gamma/(\Delta + \gamma)] - [VPD/(\Delta + \gamma)]. \quad (6)$$

Vertex 4 represents dry bare soil and $(t_s - t_a)_4$ is computed as

$$(t_s - t_a)_4 = [r_a(R_n - G)/C_v]. \quad (7)$$

Table 2 describes how values for t_a, VPD, R_n, G, r_a, r_{cp}, and r_{cx} were obtained. More detailed descriptions of how the inputs to equations (4)–(7) can be defined, and the limitations of the WDI were given by *Moran et al.* [1994, 1996].

[22] The left side of the trapezoid (cool edge) represents the theoretical range of surface temperature minus air temperature $(t_s - t_a)$ for potential evapotranspiration (ET_p) conditions. The right side (warm edge) represents the theoretical range of $t_s - t_a$ when ET = 0. When soil evaporation is close to zero, the WDI becomes a measure of transpiration (T) and is defined as

$$WDI = 1 - T/T_p = [(t_s - t_a)_m - (t_s - t_a)_r]/[(t_s - t_a)_m - (t_s - t_a)_x], \quad (8)$$

where T_p is potential transpiration and the subscripts 'm', 'x' and 'r' refer to the minimum, maximum and measured values, respectively. Theoretically, the WDI ranges from 0.0 for well watered conditions to 1.0 for maximum stress

Table 2. Origin of Input Variables Air Temperature, Vapor Pressure Deficit, Net Radiant Heat Flux Density, Soil Heat Flux Density, Canopy Resistance at Potential Evapotranspiration, Canopy Resistance Associated With Nearly Complete Stomatal Closure, and Aerodynamic Resistance Used to Generate VIT Trapezoid Vertices[a]

Input Variable	Method Obtained
t_a	measured
VPD	measured
R_n	calculated [*Jackson et al.*, 1985]
G	calculated [*Clothier et al.*, 1986]
r_{cp} and r_{cx}	calculated [*Moran et al.*, 1996]
r_a	calculated [*Brutsaert*, 1982] with stability corrections for heat and momentum [*Moran et al.*, 1994, equation (A16)]

[a]Abbreviations: origin of input variables air temperature, t_a; vapor pressure deficit, VPD; net radiant heat flux density, R_n; soil heat flux density, G; canopy resistance at potential evapotranspiration, r_{cp}; canopy resistance associated with nearly complete stomatal closure, r_{cx}; and aerodynamic resistance, r_a.

conditions, and graphically is equal to the ratio of distances AC and AB in Figure 3. WDI as a measure of transpiration (equation (8)) was the definition of WDI used for this study.

2.6. Data Selection Criteria and Calculation of Daytime Net CO_2 Flux

[23] The calculation of daytime net CO_2 flux was a two step process. The first step was to derive instantaneous net CO_2 flux (F_{ci}) using the WDI. In addition to the satellite imagery previously mentioned, data from the BREB were also utilized. The BREB data set consisted of evapotranspiration (ET) and net CO_2 flux measurements collected over the monsoon season (1 July to 31 October) for a 5-year period (1996–2000). In the Chihuahuan desert, evaporation from soil is generally small owing to infrequent rainfall events, so ET is generally dominated by plant transpiration (T) within 1 to 2 d after a storm [*Scott et al.*, 2006; *Green*, 2006]. Therefore, data for this study were limited to days that were 48 h after the most recent precipitation event, with the assumption that $E \cong 0$ and $T \cong ET$. Precipitation data from seven rain gauges throughout the study area were used to determine data selected. From these data, one data set was compiled using incoming solar radiation (R_s) to indicate clear days and another data set was compiled of days with clear mornings and cloudy afternoon conditions.

[24] To obtain a value for T_p for equation (8), the day with the highest net positive CO_2 flux at 10:20 A.M., 10:40 A.M., and 11:00 A.M. (time period listed encompasses the average flux for the previous 20 min) was determined. These times were selected because of their proximity to the time of the satellite overpasses (Table 1a). As explained earlier, only days that were two days after a storm and were determined to have day-long, clear sky conditions based on incoming solar radiation were considered. DOY 225 (13 August 1999) met the criteria and was selected. Values of T measured on DOY 225 at 10:20 A.M., 10:40 A.M. and 11:00 A.M. were used as T_p for this study (Table 2). Values of T for equation (8) were obtained for five days (Table 1a) at the time of the satellite overpass and in situ transpiration ($1-T/T_p$) values were calculated for each day using the appropriate T and T_p values. These values were used for a comparison of in situ transpiration measurements and satellite-derived WDI. A subset (15 August to 15 September) of the BREB data collected over the 5-year period was used to confirm the relation between positive F_{ci} and in situ transpiration.

[25] A modified five-band (blue, green, red, NIR, and temperature) Exotech radiometer was used to make weekly reflectance and surface temperature measurements over an 80 m radius surrounding the BREB system during the monsoon periods in 2002, 2003, 2004 and 2005. Owing to unfavorable monsoon conditions (e.g., rain or cloud cover) and periodic instrumental difficulties associated with the BREB and the Exotech, only 8 data points were considered viable. Ground-based WDI measurements were derived from this data set and used to validate the relation between F_{ci} and WDI.

[26] The second step was to calculate daytime net CO_2 flux (F_{cd}) using F_{ci}. A new data set was compiled using the 11:00 A.M. measurement for each day of the 5-year BREB data set. These data were used as F_{ci} measurements owing to their concurrence with Landsat satellite overpasses. Net CO_2 flux measurements from 6:00 A.M. to 6:00 P.M. were also summed and used as actual F_{cd} for each day. This new data set, consisting of 110 d, was randomly split to form two separate data sets. The first set contained 51 d and was used to examine the relationship between F_{ci} and F_{cd}. The second set of 59 d was used for validation of the relation. The resulting equation from that comparison was applied to Landsat imagery to generate spatial maps of F_{cd}.

2.7. Nighttime and Daytime Flux Data Sets

[27] Nighttime net CO_2 flux (F_{cn}) data were collected using the automated chamber, converted to corrected data (F_{cac}) using a scaling factor, and summed over the period from 6:00 P.M. to 6:00 A.M. during the monsoon growing season (1 June to 31 October) in 2005 and 2006. Days were screened for cloud cover using incoming solar radiation data from the meteorological station located within the study area. Only days completely free of clouds, or clear during the time period between 10:00 A.M. and 11:00 A.M. were used. Daytime net CO_2 flux (F_{cd}) data were derived from BREB data summed over the time period from 6:00 A.M. to 6:00 P.M. on days coinciding with the nighttime data set. To ensure that soil moisture conditions were the same during both the daytime and nighttime periods, precipitation data from the seven rain gauges throughout the study area were examined and days that had experienced rainfall were excluded. This data set containing 68 d was randomly split to form two separate data sets. The first set containing 35 d was used to examine the relationship between daytime and nighttime flux. The second set of 33 d was used for validation of the relation.

3. Results and Discussion

[28] The first portion of this study, the estimation of distributed F_{cd}, was based on the first two objectives: (1) to derive F_{ci} using the WDI, and (2) to estimate F_{cd} from the WDI-derived F_{ci}. The third objective, to derive the relation between daytime and nighttime net CO_2 flux, was addressed in the second portion of the study. The following subsections discuss the results of this study in regard to these objectives, as well as the final product maps of distributed total daily net CO_2 flux.

3.1. Estimation of Instantaneous CO_2 Flux From WDI

[29] To generate a relation to estimate F_{ci} from the WDI, it was first necessary to show that the WDI was a measure of transpiration (equation (8)). Therefore, WDI measurements derived from satellite imagery (Table 1a) were compared to in situ transpiration measurements collected by the BREB system on corresponding days. The result was the exponential relation

$$\mathrm{WDI} = -0.6475 + \left(0.6475 * \exp^{(0.9339(1-T/Tp))}\right), \qquad (9)$$

where ($1 - T/T_p$) is in situ transpiration (Figure 4). According to *Holifield et al.* [2003], the relationship is exponential, rather than linear as indicated by equation (8), because WDI does not account for sensible heat transfer between warm soil and cool vegetation that results in an increase in canopy T when surface heterogeneity is greatest (partial-cover vegetation cover conditions). However, considering the differences in scale and the potential error in both measurement approaches, an index of agreement

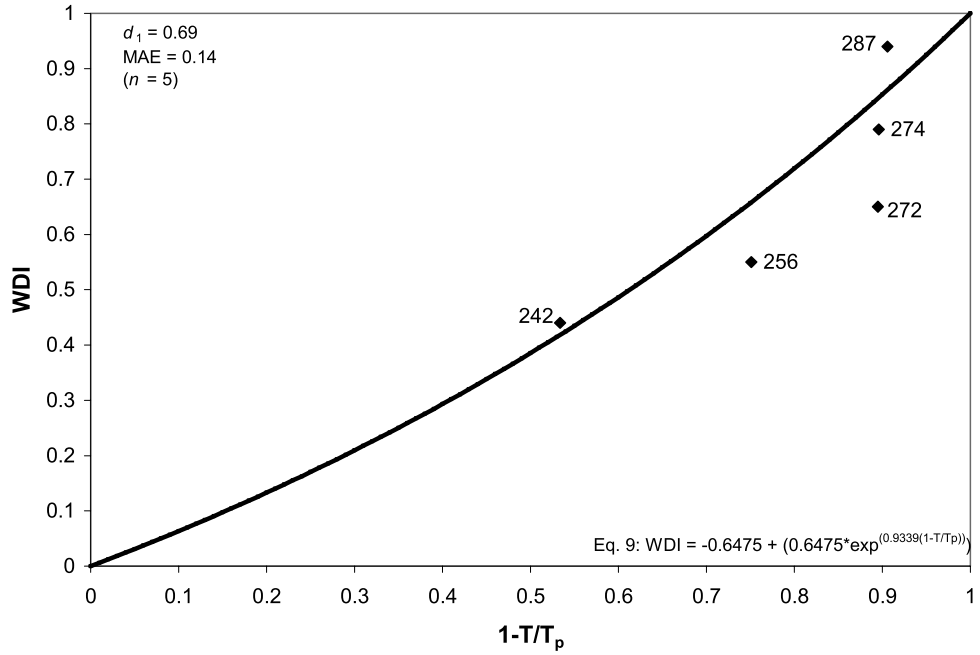

Figure 4. Comparison of satellite derived water deficit index (WDI) and in situ (actual (T) and potential (T_p)) transpiration measurements for 14 October 1997 (DOY 287), 30 August 1998 (DOY 242), 1 October 1998 (DOY 274), 12 September 2000 (DOY 256), and 28 September 2000 (DOY 272). Index of agreement (d_1) and mean absolute error (MAE) are presented.

(d_1) [*Legates and McCabe*, 1999] of 0.69 and a mean absolute error (MAE) of 0.14 indicated the relation was good and supported the use of WDI for estimating transpiration.

[30] The next step was to verify the inherent relationship that exists between positive F_{ci}, which is dominated by plant uptake, and in situ transpiration. Namely, as plant CO_2 uptake increases, transpiration also increases. This comparison was done using the subset of BREB data for the monsoon period of 15 August to 15 September for 1996–2000. This time period was chosen to ensure that the vegetation at the site would be in the midst of its active growth period. During this time, green vegetation is present

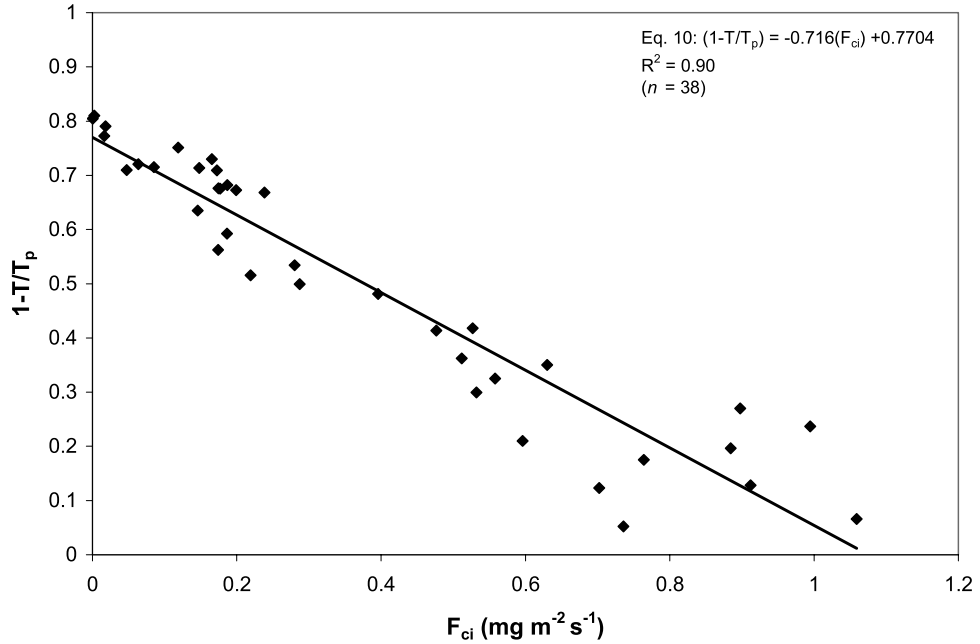

Figure 5. Comparison of positive instantaneous net CO_2 flux (F_{ci}) (dominated by plant uptake) and in situ (actual (T) and potential (Tp)) transpiration for the summer monsoon period of 15 August to 15 September for 1996–2000.

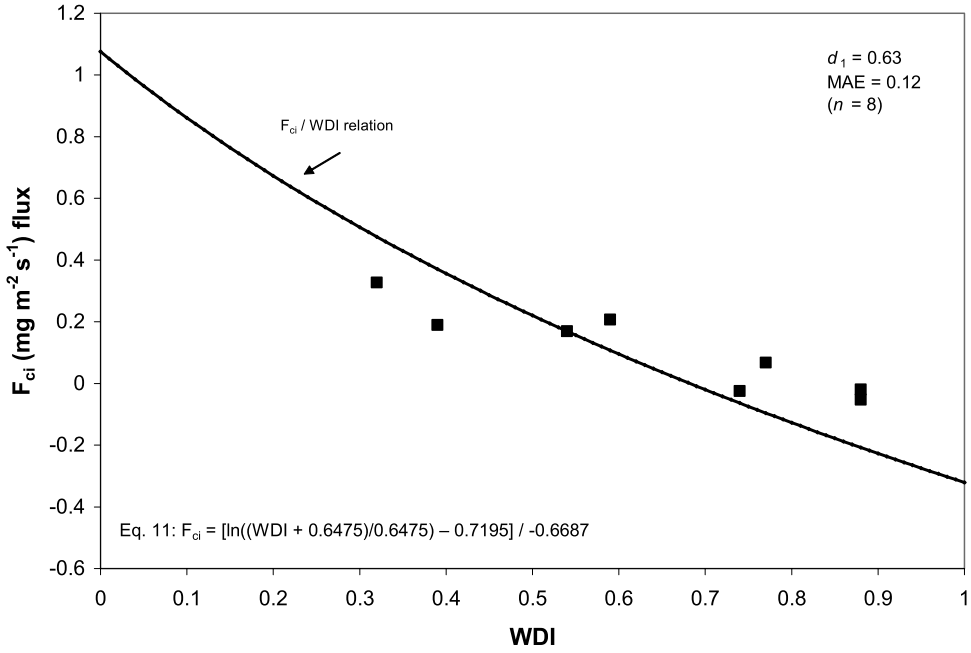

Figure 6. Comparison of instantaneous net CO_2 flux (F_{ci}) and water deficit index (WDI). Validation for the relation was performed using WDI data collected in 2002, 2003, 2004, and 2005 by an Exotech radiometer. Index of agreement (d_1) and mean absolute error (MAE) are presented.

and actively transpiring and photosynthesizing. The result was the linear relation

$$\left(1 - T/T_p\right) = -0.716(F_{ci}) + 0.7704, \quad (10)$$

where F_{ci} is instantaneous net CO_2 flux (Figure 5). Although, some increased scatter is seen with higher transpiration rates, the relation was very strong with an R^2 of 0.90.

[31] Last, equations (9) and (10) were combined to produce the equation

$$F_{ci} = [\ln((WDI + 0.6475)/0.6475) - 0.7195]/ -0.6687, \quad (11)$$

which represents a relationship between WDI and instantaneous net CO_2 flux. This exponential relationship was validated using ground data collected with the Exotech radiometer (Figure 6). The data collected with the Exotech radiometer, a surrogate for satellite data, were used to derive the WDI values used for the validation. The index of agreement between measured and WDI-derived instantaneous net CO_2 flux was 0.63, with an MAE of 0.12 mg m^{-2} s.

3.2. Estimation of Daytime CO_2 Flux From Instantaneous Flux

[32] Determining a method for estimating F_{cd} from F_{ci} was the second objective of this study. According to *Jackson et al.* [1983], plant ET produces a curve similar to measured incoming solar radiation (R_s) under clear sky conditions (Figure 7a), when soil water availability is unlimited, as in the case of irrigated agricultural fields. To a certain extent this was found to be true even under the water limited conditions found in semiarid grasslands (Figures 7b–7d). Although faint owing to the noisy nature of the data, the same curvature exhibited by the R_s was evident in the transpiration measurements. It was also apparent that as VPD increases, transpiration will increase as long as the soil water condition can support the plant water demands. For example, the VPD for 23 September 1998 was higher than that of 21 August 1999, however it only had about half of the August date's soil water content, causing considerably less transpiration to occur. On the basis of the linear relationship that exists between positive F_{ci} and transpiration (Figure 5), a curve similar to that of R_s was expected for positive F_{ci}. Unfortunately, this did not occur (Figure 7e). On days when transpiration was very high and soil water was not limiting, F_{ci} did have the expected curvature. However, in cases when water was limited, instead of having the very slight curvature expressed by transpiration, F_{ci} was essentially flat. There were also instances observed when F_{ci} would peak in the morning (e.g., 10 or 11:00 A.M.) then sharply fall and become a flat line for the rest of the day (data not shown). Still, the trend in F_{ci} flux observed at 11:00 A.M. proved to be a strong indicator of the flux trend for the entire daytime period (Figure 8a), providing the link needed to obtain daytime flux values from an instantaneous measure.

[33] The data set containing F_{ci} measurements collected by the BREB at 11:00 A.M. were compared to the F_{ci} values summed over the 6:00 A.M. to 6:00 P.M. period, in order to determine the relationship between F_{ci} and F_{cd} (Figure 8a). The result was the strong (R^2 = 0.97) linear relation

$$F_{cd} = 25.334(F_{ci}) + 0.0446, \quad (12)$$

where F_{cd} is daytime net CO_2 flux and F_{ci} is instantaneous net CO_2 flux. The relation was validated using data from 1996 to 2000 (Figure 8b). The mean absolute error (MAE) for the net negative (loss from ecosystem) and positive flux

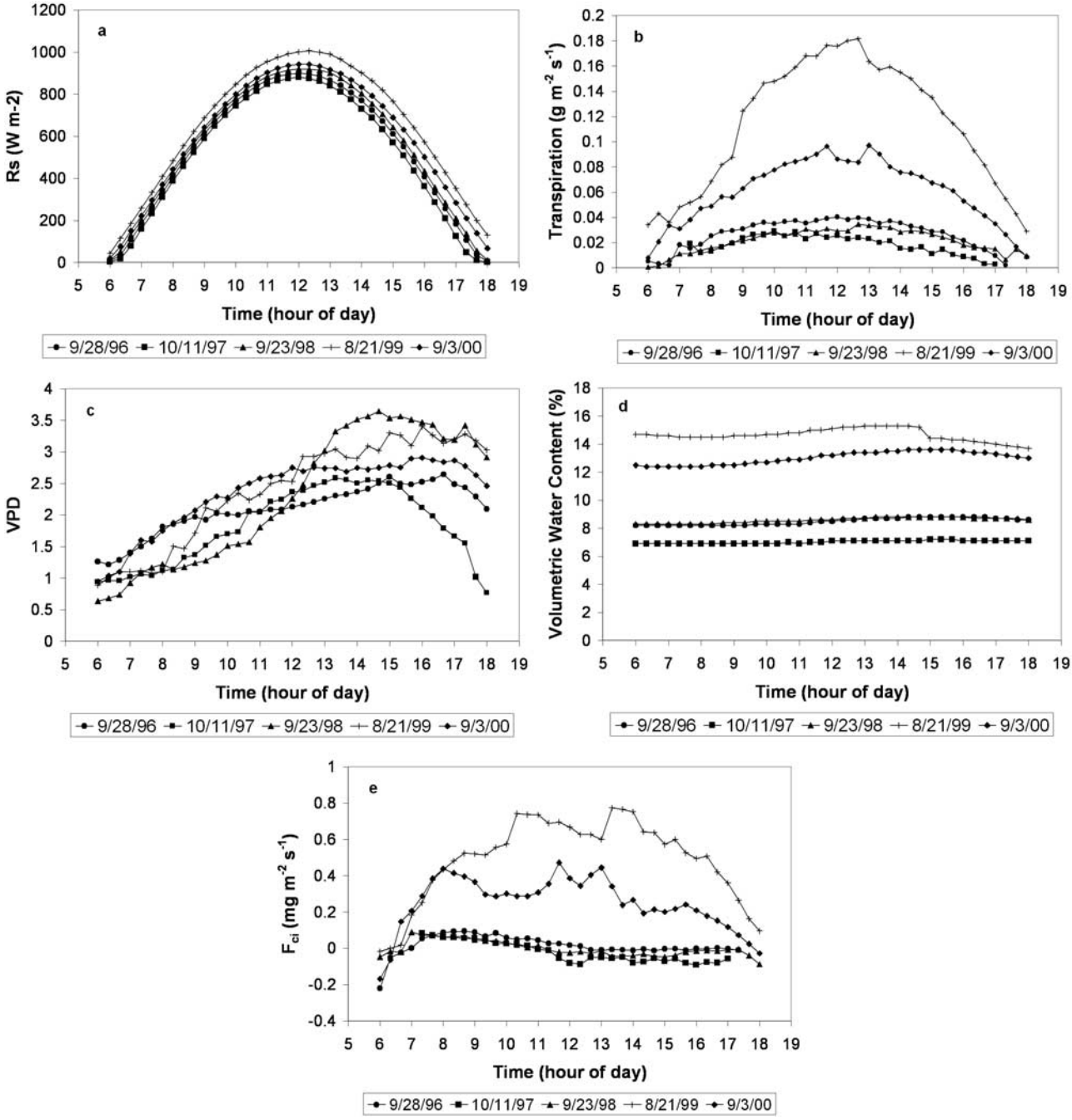

Figure 7. (a) Examples of measured incoming solar radiation (R_s) from 6:00 A.M. to 6:00 P.M. under cloud-free conditions. Measurements of (b) transpiration, (c) vapor pressure deficit (VPD), and (d) volumetric water content under cloud-free conditions. (e) Measurements of instantaneous net CO_2 flux (F_{ci}) for cloud-free days with varying plant water availability.

values were 0.46 g m^{-2} (12 h)$^{-1}$ and 1.14 g m^{-2} (12 h)$^{-1}$ respectively.

[34] Analysis was also done to determine what happens to F_{cd} when a day has a clear morning, but clouds appear in the afternoon (Figure 9a). This scenario is more typical of atmospheric conditions during the monsoon growing season. The relationship remained linear when the net flux was negative. This was apparently due to the fact that soil moisture is the limiting factor when negative net CO_2 flux occurs. As a result, it made no difference whether sky conditions were clear or cloudy because the water limitation dominated. However, when the net flux was high and positive, the relationship became slightly curvilinear. When net flux is positive, water is generally not a limiting factor. In these instances, R_s becomes the limiting factor. When cloudy conditions occurred, F_{cd} flux began to decrease as plants were forced to limit photosynthesis, causing a decrease in positive flux. Consequently, when equation (12) was applied using the F_{ci} values for these days, the result was an overestimation of F_{cd} (Figure 9b), with MAEs of

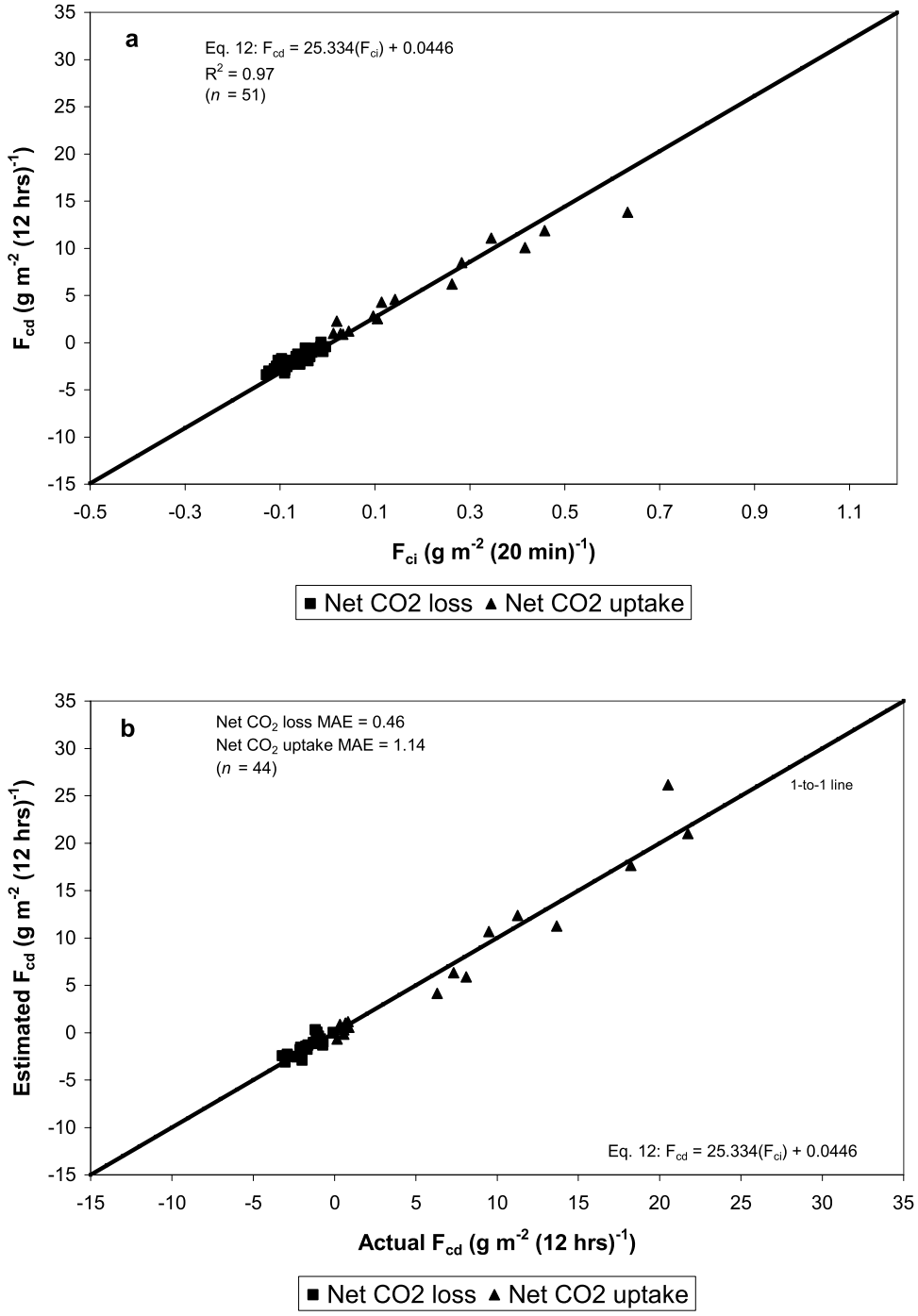

Figure 8. (a) Comparison of daytime (F_{cd}) and 11:00 A.M. instantaneous (F_{ci}) net CO_2 flux on clear days. (b) Comparison of estimated and actual daytime net CO_2 flux. Negative flux values indicate net CO_2 loss from the soil. Positive values indicate net CO_2 uptake by plants. Mean absolute error (MAE) is presented.

0.58 g m^{-2} (12 h)$^{-1}$ and 1.73 g m^{-2} (12 h)$^{-1}$ respectively for net negative and positive flux.

3.3. Estimation of Nighttime Net CO_2 Flux From Daytime Flux Estimates

[35] Manual collar measurements were compared with automated chamber measurements. Although both systems of measurement followed the same trend, collar measurements were always greater than measurements from the chamber (Figure 10). This was most likely due to the chamber's placement on the ridge top where flux rates tended to be small, which created a bias of underestimation in measurements collected by the automated chamber. Collars were placed both along the ridge top and on the slopes on either side to obtain a more complete picture of soil respiration throughout the landscape. Therefore, in

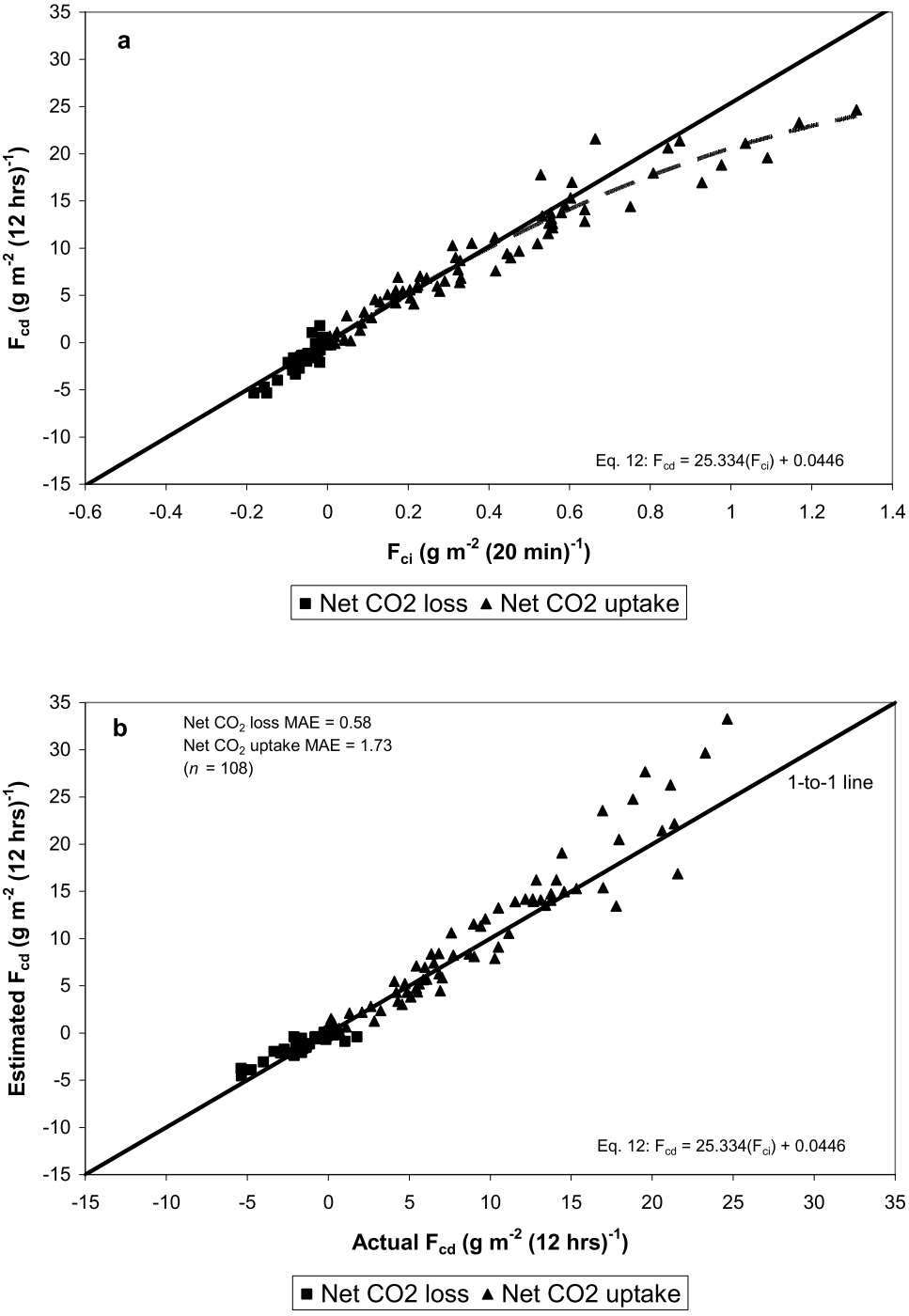

Figure 9. (a) Comparison of daytime (F_{cd}) and 11:00 A.M. instantaneous (F_{ci}) net CO_2 flux for days with clear mornings and cloudy afternoons. The dashed line follows the curve created by the net CO_2 uptake values. (b) Comparison of estimated and actual daytime net CO_2 flux for days with clear mornings and cloudy afternoons. Negative and positive flux values indicate net CO_2 loss and uptake, respectively. Mean absolute error (MAE) is presented.

order to make use of the extended temporal scale provided by the automated chamber, and the spatial influence captured by the collars, chamber and collar data were plotted against one another and a linear relationship was found (Figure 11, $R^2 = 0.88$). This linear relation

$$F_{cac} = 1.9134(F_{ca}), \quad (13)$$

where F_{ca} is data collected by the automated chamber, was used to produce corrected chamber flux measurements (F_{cac}) which accounted for the spatial variability of soil respiration within the study area.

[36] To determine the relationship between F_{cd} and F_{cn}, daytime and nighttime flux were plotted against each other

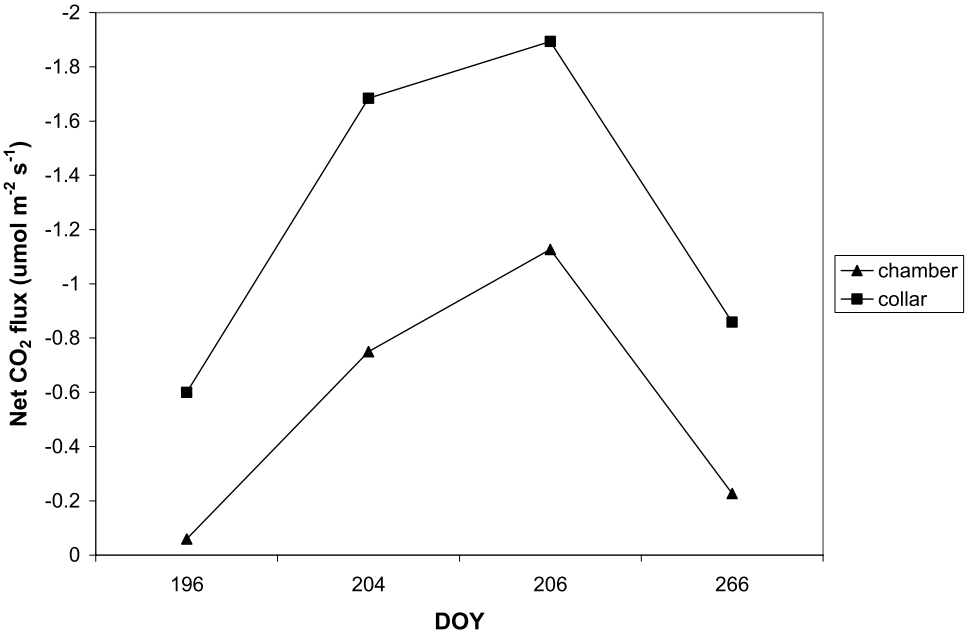

Figure 10. Comparison of automated chamber measurements and manual collar measurements of net CO_2 flux for four days (15 July (DOY 196), 23 July (DOY 204), 25 July (DOY 206), and 23 September (DOY 266)) during the nighttime period from 8:00 P.M. to 12:00 A.M. in 2005.

(Figure 12a) and a linear relation was found ($R^2 = 0.88$). This relation

$$F_{cn} = -0.2035(F_{cd}) - 0.5989 \quad (14)$$

where F_{cd} is daytime net CO_2 flux, was applied to the second data set for validation and a very strong relationship was found (Figure 12b, MAE = 0.31). Nighttime respiration is influenced by photosynthetic activity that has occurred during the day. When plants were active, as indicated by positive net CO_2 flux values, nighttime flux values were higher. This is most likely caused by the increase in root exudates, which provide the carbon based energy needed by soil microorganisms. In addition, positive net flux is an indicator of transpiration activity, which implies an adequate soil moisture condition. Adequate soil moisture

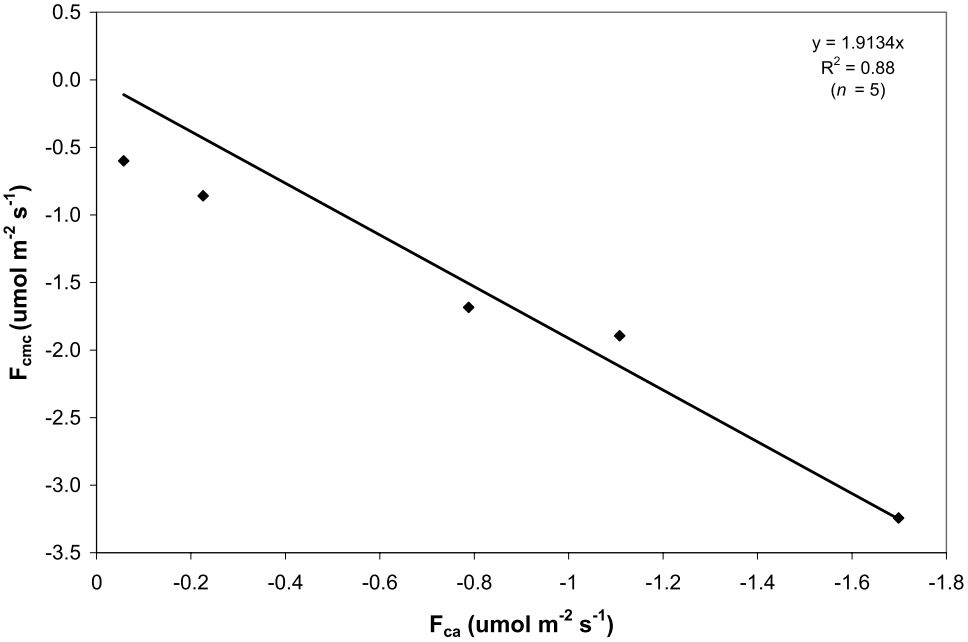

Figure 11. Comparison of automated chamber net CO_2 flux (F_{ca}) data to manually collected collar net CO_2 flux (F_{cmc}) data for 5 d in 2005. Negative flux values indicate net CO_2 loss from the soil.

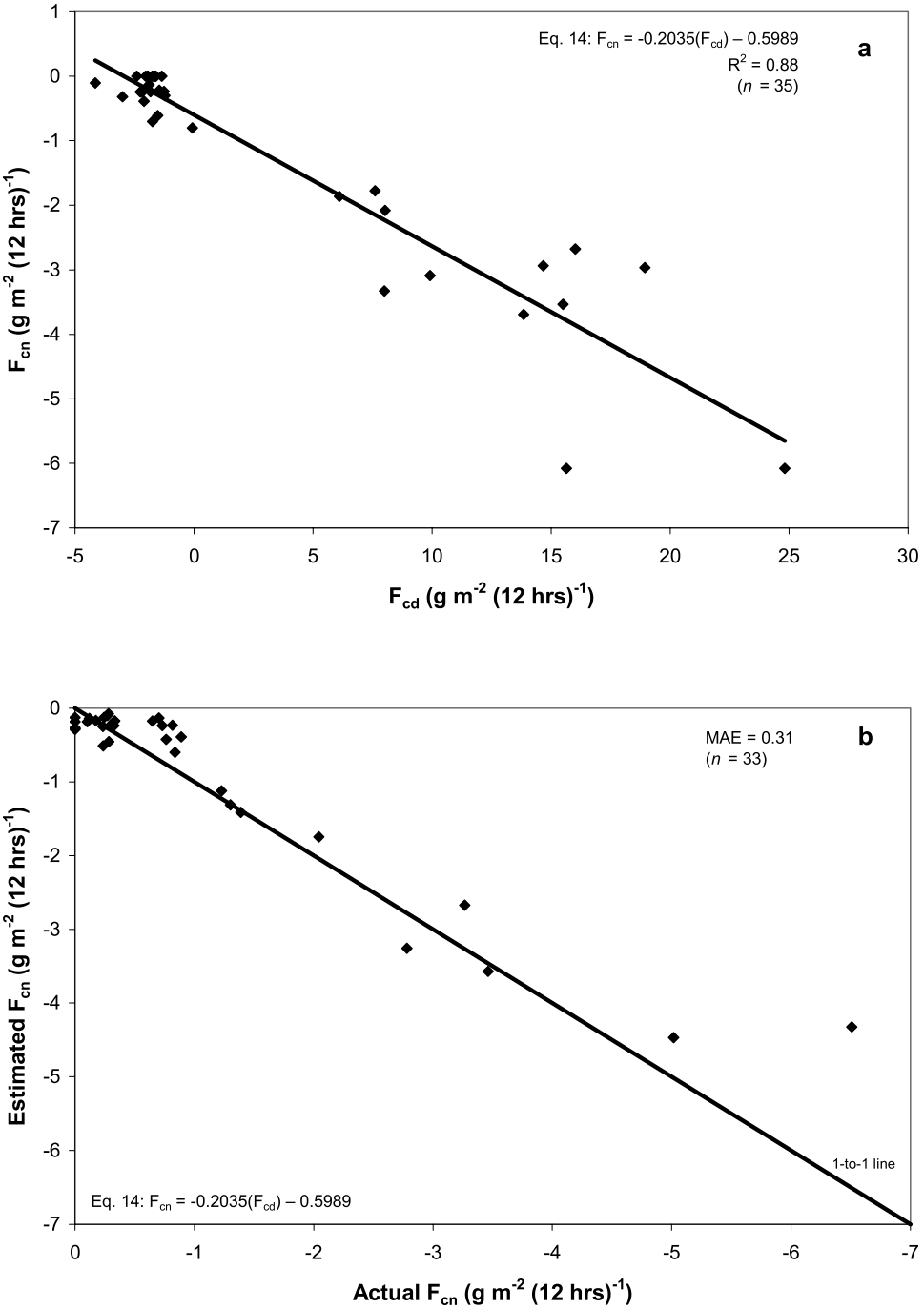

Figure 12. (a) Comparison of daytime (F_{cd}) and nighttime (F_{cn}) net CO_2 flux. (b) Comparison of estimated and actual nighttime net CO_2 flux. Negative flux values indicate net CO_2 loss from the soil. Positive values indicate net CO_2 uptake by plants. Mean absolute error (MAE) is presented.

also contributes to microbial activity and can result in higher nighttime flux rates.

3.4. Distributed Daily Net CO_2 Flux

[37] Maps of F_{cd} and F_{cn} for days from 7 years spanning from 1990 to 2000 were generated over the 9 km^2 study area by applying equations (12) and (14) to Landsat satellite imagery. These maps were then combined as

$$F_{ct} = F_{cd} + F_{cn} \quad (15)$$

to create maps of total daily net CO_2 flux (F_{ct}) (Figure 13). Through this method of estimating distributed F_{ct}, it was possible to determine daily fluxes over the area before BREB instrumentation was installed within the watershed (Figures 13a–13g).

[38] These daily maps of total net CO_2 flux supported the finding by *Emmerich* [2003] that semiarid grasslands can serve as both a sink and a source of atmospheric CO_2. The examples presented in Figure 13, with the exception of Figure 13b, tended to depict the semiarid grassland site as a

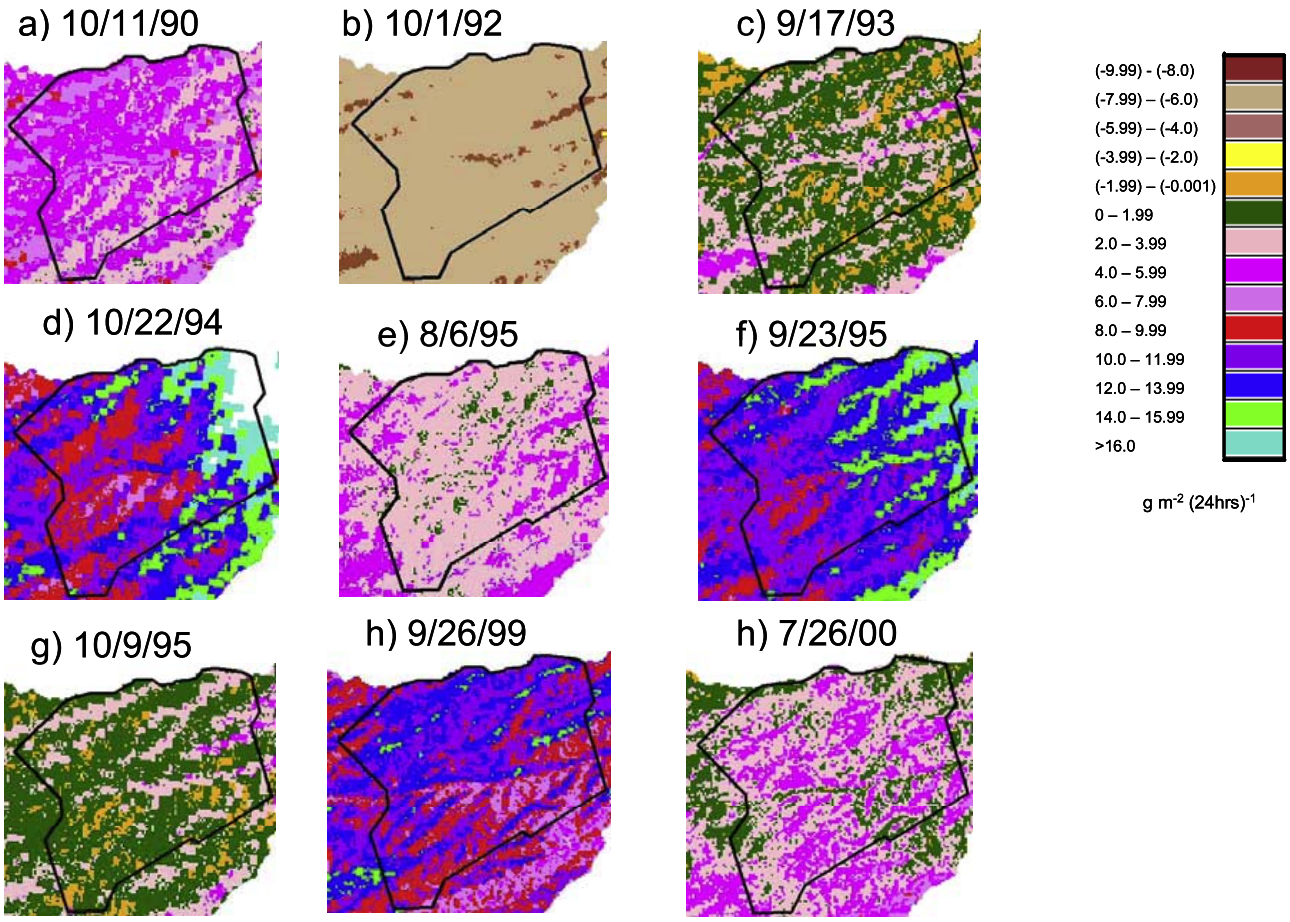

Figure 13. Seven years of Landsat images of total daily net CO_2 flux (g m^{-2} (24 h)$^{-1}$) over the 9 km^2 study area. Negative values indicate net CO_2 loss from the soil. Positive values indicate net CO_2 uptake by plants.

sink. In Figure 13b, the monsoon rains had shut down by the end of August and the rainfall in September only averaged 6.9 mm over the entire study area. By the time the 1 October scene was taken, there was very little, if any, CO_2 uptake occurring making this site a net source rather than a sink for CO_2. However, there were also instances when the study site served as both sink and source simultaneously (Figures 13c and 13g). The scenes from 1995 (Figures 13e–13g) provided the ability to view the spatial changes in net CO_2 flux that occurred through the progression of an entire monsoon period. These figures marked changes from the point where uptake had begun to surpass loss from the soil (Figure 13e), to the peak in photosynthetic activity characterized by very high CO_2 uptake (Figure 13f), to the move toward the point where CO_2 loss from the soil began to exceed uptake (Figure 13g).

[39] The spatial variability of net CO_2 flux could often be attributed to soil moisture differences caused by localized storm activity occurring within the watershed. Figures 13h and 13d were very good examples of a fairly common scenario. On 22 September 1999, four days before the scene depicted in Figure 13h was taken, a very large storm occurred. This storm dropped a spatial average of 27.9 mm of rainfall over the study area. However, the upper portion

Table 3. Error Analysis Results[a]

DOY	Mean WDI and STD	F_{ci} and SE, equation (11), g m^{-2} (20 min)$^{-1}$	F_{cd} and SE, equation (12), g m^{-2} (12 h)$^{-1}$	F_{cn} and SE, equation (14) g m^{-2} (12 h)$^{-1}$	F_{ct} and SE, equation (15), g m^{-2} (24 h)$^{-1}$
287_97	0.95 (±) 0.08	−0.28 (±) 0.12	−7.02 (±) 3.10	0.83 (±) 0.65	−6.19 (±) 3.16
242_98	0.48 (±) 0.05	0.25 (±) 0.21	6.43 (±) 5.31	−1.91 (±) 1.09	4.52 (±) 5.42
274_98	0.73 (±) 0.08	−0.06 (±) 0.14	−1.38 (±) 3.60	−0.32 (±) 0.74	−1.70 (±) 3.68
256_00	0.52 (±) 0.07	−0.20 (±) 0.21	5.13 (±) 5.25	−1.64 (±) 1.07	3.49 (±) 5.36
272_00	0.54 (±) 0.06	0.16 (±) 0.19	4.19 (±) 4.93	−1.46 (±) 1.01	2.74 (±) 5.03
n	10,000	43	51	35	86
Data range		(−0.32)-1.08	(−3.40)-13.81	(−6.08)-(−0.10)	(−6.08)-13.81

[a]Mean water deficit index (WDI) and standard deviation (STD) values, as well as instantaneous net CO_2 flux (F_{ci}), daytime net CO_2 flux (F_{cd}), nighttime net CO_2 flux (F_{cn}), total daily net CO_2 flux (F_{ct}) and their standard errors (SE), are presented for five satellite dates.

of the study area received 35% more rain from the storm than the lower portion. This spatial variability was in turn reflected in the CO_2 flux map. In Figure 13d, the last storm that occurred within the study area was on 16 October 1994. The monsoon period in 1994 was very wet, with an average rainfall of 214.4 mm for the entire study area. There was plenty of water available to support transpiration, thus net uptake of CO_2 was very high for the day, reaching >16.0 g m^{-2} (24 h)$^{-1}$ in several places within the study area. It should be noted that the white areas within this scene were due to some of the measured values of $(t_s - t_a)$ slightly exceeding the cool edge of the VIT Trapezoid, causing WDI to be less than zero. This type of discrepancy can often be caused by error in the satellite sensor calibration, over- or under-correction of the remotely sensed data for atmospheric conditions, or by errors associated with calculating the warm and cool edges [*Holifield et al.*, 2003].

3.5. Error Analysis

[40] An analysis of the error associated with the daily net CO_2 flux values produced using this approach was conducted. A Monte Carlo model created in MatLab® was run for 10,000 iterations while the WDI inputs (R_s, t_s, t_a, SAVI, wind speed, and relative humidity) were varied to their reasonable minimums and maximums. These estimates of the measurement uncertainty (to 95% confidence), as indicated by *Moran* [1990], were based on ideal conditions where all instruments were operating to specifications.

[41] The mean WDI and standard deviation values from the Monte Carlo runs for the five satellite dates used to develop equation (9) (Table 3) were used to conduct the error analysis.

[42] Parameter estimation and generation of the uncertainty matrices for equations (9), (10), (12), and (14) were performed using the Marquardt-Levenberg [*Seber and Wild*, 2003] and Least Squares methods. The Marquardt-Levenberg and Least Squares methods were used to determine the model parameter vector β and the uncertainty matrix σ^2 in the parameters for equation (9). The Least Squares method was used to determine β and σ^2 for equations (10), (12), and (14). A MatLab® program was developed to compute the values of β and σ^2 for all the parameters. The error propagation was then carried out using the First Order Taylor Series [*Bevington and Robinson*, 1992]. The results of the error propagation are presented in Table 3. All standard errors for the error propagation, with the exception of DOY 287, fell within the range of the data used to develop each of the relationships for the modeling approach. The approach was found to be viable over essentially the whole range of WDI values (0–0.9). However, when very high WDI values (>0.9) are present, the model may not work very well owing to extremely low transpiration rates.

4. Conclusions

[43] There was a curvilinear relationship between in situ transpiration measurements and satellite-derived WDI measurements of transpiration. When combined with the strong linear relation found between in situ transpiration and positive net CO_2 flux, it was possible to estimate instantaneous net CO_2 flux from a WDI at 11:00 A.M. Further, a strong linear relationship was discovered between net CO_2 flux at 11:00 A.M. and net daytime flux. As a result, it was possible to apply this relation to Landsat satellite imagery and create maps of distributed daytime net CO_2 flux. There were strong linear relationships between data collected using the manual and automatic chambers, and between daytime and nighttime net CO_2 flux. Satellite-derived maps of daytime net CO_2 flux were used to obtain nighttime net CO_2 flux. These maps of daytime and nighttime flux were combined to generate maps of total daily net CO_2 flux. This approach for estimating daily net CO_2 flux was operational over a wide range of values for WDI (0 to 0.9).

[44] Remote sensing in combination with a micrometeorological method (BREB or EC) of measuring carbon and water fluxes, has great potential as a tool for better understanding the role of semiarid grasslands in the carbon cycle. This study showed it was possible to obtain reasonable distributed estimates of daily net CO_2 flux at the landscape scale for semiarid grasslands during periods when plants are actively transpiring. In addition, it served to support the previous finding by *Emmerich* [2003] that these grasslands serve not only as a sink, but as an important source of CO_2, and further, demonstrated the spatial variability of CO_2 flux, emphasizing the need for measurements capable of capturing that variability. Future work will be focused on determining seasonal patterns of daily net CO_2 flux and annual net CO_2 flux in semiarid grasslands.

[45] **Acknowledgments.** This research was supported by the NASA EO-1 Validation Team, grant S-10217-X. The authors wish to express sincere thanks to the personnel at the USDA-ARS Southwest Watershed Research Center, Tucson, and the USDA-ARS Tombstone facility, Kittipat "Bot" Kampa from the University of Florida, Adolfo Diaz Gutierrez from Cordoba University, Spain, and Jared Buono, Ryan Manon, and Christina Contreras from the University of Arizona for their cooperation and assistance. Mention of proprietary product does not constitute a guarantee or warranty of the product by USDA or the author and does not imply its approval to the exclusion of other products that may also be suitable.

References

Bachelet, D., R. P. Neilson, J. M. Lenihan, and R. J. Drapek (2001), Climate change effects on vegetation distribution and carbon budget in the United States, *Ecosystems*, *4*, 164–185, doi:10.1007/s10021-001-0002-7.

Baldocchi, D. D., and K. B. Wilson (2001), Modeling CO_2 and water vapor exchange of a temperate broadleaf forest across hourly and decadal time scales, *Ecol. Modell.*, *142*, 155–184, doi:10.1016/S0304-3800(01)00287-3.

Baldocchi, D., et al. (2001), FLUXNET: A new tool to study the temporal and spatial variability of ecosystem scale carbon dioxide, water vapor and energy flux densities, *Bull. Am. Meteorol. Soc.*, *82*, 2415–2434, doi:10.1175/1520-0477(2001)082<2415:FANTTS>2.3.CO;2.

Bevington, P. R., and D. K. Robinson (1992), *Data Reduction and Error Analysis for the Physical Sciences*, 328 pp., McGraw-Hill, New York.

Box, E. O., B. N. Holben, and V. Kalb (1989), Accuracy of the AVHRR vegetation index as a predictor of biomass, primary productivity and net CO_2 flux, *Vegetatio*, *80*, 71–89, doi:10.1007/BF00048034.

Brutsaert, W. H. (1982), *Evaporation Into the Atmosphere*, D. Reidel, London.

Buchmann, N. (2000), Biotic and abiotic factors controlling soil respiration rates in *Picea abies* stands, *Soil Biol. Biochem.*, *32*, 1625–1635, doi:10.1016/S0038-0717(00)00077-8.

Clothier, B. E., K. L. Clawson, P. J. Pinter Jr., M. S. Moran, R. J. Reginato, and R. D. Jackson (1986), Estimation of soil heat flux from net radiation during the growth of alfalfa, *Agric. For. Meteorol.*, *37*, 319–329, doi:10.1016/0168-1923(86)90069-9.

Colaizzi, P. D., E. M. Barnes, T. R. Clarke, C. Y. Choi, P. M. Waller, J. Haberland, and M. Kostrzewski (2003), Water stress detection under high frequency sprinkler irrigation with water deficit index, *J. Irrig. Drain. Eng.*, *129*(1), 36–43, doi:10.1061/(ASCE)0733-9437(2003)129:1(36).

Davidson, E. A., K. Savage, L. V. Verchot, and R. Navarro (2002), Minimizing artifacts and biases in chamber-based measurements of soil respiration, *Agric. For. Meteorol.*, *113*, 21–37, doi:10.1016/S0168-1923(02)00100-4.

Dugas, W. A. (1993), Micrometeorological and chamber measurements of CO_2 flux from bare soil, *Agric. For. Meteorol.*, *67*, 115–128, doi:10.1016/0168-1923(93)90053-K.

Dugas, W. A., M. L. Heuer, and H. S. Mayeux (1999), Carbon dioxide fluxes over bermudagrass, native prairie, and sorghum, *Agric. For. Meteorol.*, *93*, 121–139, doi:10.1016/S0168-1923(98)00118-X.

Emmerich, W. E. (2003), Carbon dioxide fluxes in semiarid environment with high carbonate soils, *Agric. For. Meteorol.*, *116*, 91–102, doi:10.1016/S0168-1923(02)00231-9.

Frank, A. B., and W. A. Dugas (2001), Carbon dioxide fluxed over a northern, semiarid, mixed-grass prairie, *Agric. For. Meteorol.*, *108*, 317–326, doi:10.1016/S0168-1923(01)00238-6.

Franzluebbers, K., A. J. Franzluebbers, and M. D. Jawson (2002), Environmental controls on soil and whole-ecosystem respiration from a tallgrass prairie, *Soil Sci. Soc. Am. J.*, *66*, 254–262.

Gilmanov, T. G., L. L. Tieszen, B. K. Wylie, L. B. Flanagan, A. B. Frank, M. R. Haferkamp, T. P. Meyers, and J. A. Morgan (2005), Integration of CO_2 flux and remotely-sensed data for primary production and ecosystem respiration analyses in the Northern Great Plains: Potential for quantitative spatial extrapolation, *Global Ecol. Biogeogr.*, *14*, 271–292, doi:10.1111/j.1466-822X.2005.00151.x.

Green, K. N. (2006), Partitioning of evapotranspiration in a Chihuahuan Desert grassland, M.S. thesis, 102 pp., Univ. of Ariz., Tucson.

Holifield, C. D., S. McElroy, M. S. Moran, R. Bryant, T. Miura, and W. E. Emmerich (2003), Temporal and spatial changes in grassland transpiration detected using Landsat TM and ETM+ imagery, *Can. J. Remote Sens.*, *29*(2), 259–270.

Huete, A. R. (1988), A soil-adjusted vegetation index (SAVI), *Remote Sens. Environ.*, *27*, 47–57.

Huxman, T. E., J. M. Cable, D. D. Ignace, J. A. Eilts, N. B. English, J. Weltzin, and D. G. Williams (2004), Response of net ecosystem gas exchange to a simulated precipitation pulse in a semi-arid grassland: The role of native versus non-native grasses and soil texture, *Oecologia*, *141*, 295–305.

Intergovernmental Panel on Climate Change (2005), *IPCC Special Report on Carbon Dioxide Capture and Storage*, edited by E. Calvo and E. Jochem, Cambridge Univ. Press, Cambridge, U. K.

Jackson, R. D., S. B. Idso, R. J. Reginato, and P. J. Pinter Jr. (1981), Canopy temperature as a crop water stress indicator, *Water Resour. Res.*, *17*, 1133–1138, doi:10.1029/WR017i004p01133.

Jackson, R. D., J. L. Hatfield, R. J. Reginato, S. B. Idso, and P. J. Pinter Jr. (1983), Estimation of daily evapotranspiration from one time-of-day measurements, *Agric. Water Manage.*, *7*, 351–362, doi:10.1016/0378-3774(83)90095-1.

Jackson, R. D., P. J. Pinter Jr., and R. J. Reginato (1985), Net radiation calculated from remote multispectral and ground station meteorological data, *Agric. For. Meteorol.*, *35*, 153–164, doi:10.1016/0168-1923(85)90081-4.

Lafont, S., L. Kergoat, G. Dedieu, A. Chevillard, U. Karstens, and O. Kolle (2002), Spatial and temporal variability of land CO_2 fluxes estimated with remote sensing and analysis data over western Eurasia, *Tellus, Ser. B*, *54*, 820–833.

Lansing, J. C., and J. L. Barker (1985), Thermal band characterization of the Landsat-4 thermatic mapper, in *Proceedings of the Landsat-4 Science Characterizations Early Results Symposium*, edited by J. L. Barker, pp. 233–256, *Conf. Publ. CP-2355*, NASA, Washington, D. C.

Legates, D. R., and G. J. McCabe Jr. (1999), Evaluating the use of "goodness-of-fit" measures in hydrologic and hydroclimatic model validation, *Water Resour. Res.*, *35*(1), 233–241, doi:10.1029/1998WR900018.

Lim, C., M. Kafatos, and P. Megonigal (2004), Correlation between atmospheric CO_2 concentration and vegetation greenness in North America: CO_2 fertilization effect, *Clim. Res.*, *28*, 11–22, doi:10.3354/cr028011.

Monteith, J. L. (1973), *Principles of Environmental Physics*, Edward Arnold, London.

Moran, M. S. (1990), A satellite-based approach for evaluation of the spatial distribution of evapotranspiration from agricultural lands, Ph.D. dissertation, 223 pp., Univ. of Ariz., Tucson.

Moran, M. S. (1994), Irrigation management in Arizona using satellites and airplanes, *Irrig. Sci.*, *15*, 35–44, doi:10.1007/BF00187793.

Moran, M. S., T. R. Clarke, Y. Inoue, and A. Vidal (1994), Estimating crop water deficit using the relation between surface-air temperature and spectral vegetation index, *Remote Sens. Environ.*, *49*, 246–263, doi:10.1016/0034-4257(94)90020-5.

Moran, M. S., A. F. Rahman, J. C. Washburne, D. C. Goodrich, M. A. Weltz, and W. P. Kustas (1996), Combining the Penman-Monteith equation with measurements of surface temperature and reflectance to estimate evaporation rates of semiarid grassland, *Agric. For. Meteorol.*, *80*, 87–109, doi:10.1016/0168-1923(95)02292-9.

Moran, M. S., R. Bryant, K. Thome, W. Ni, Y. Nouvellon, M. P. Gonzalez-Dugo, J. Qi, and T. R. Clarke (2001), A refined empirical line approach for reflectance factor retrieved from Landsat-5 TM and Landsat-7 ETM+, *Remote Sens. Environ.*, *78*, 71–82, doi:10.1016/S0034-4257(01)00250-4.

Niemeijer, D., J. Puigdefabregas, R. White, R. Lal, M. Winslow, J. Ziedler, S. Prince, E. Archer, and C. King (2005), Dryland systems, in *Ecosystems and Human Well-Being: Current State and Trends*, vol. 1, edited by Millennium Ecosystem Assessment, chap. 22, pp. 623–662, Island, Washington, D. C.

Novick, K. A., P. C. Stoy, G. G. Katul, D. S. Ellsworth, M. B. S. Siqueira, J. Juang, and R. Oren (2004), Carbon dioxide and water vapor exchange in a warm temperate grassland, *Oecologia*, *138*, 259–274, doi:10.1007/s00442-003-1388-z.

Potts, D. L., T. E. Huxman, J. M. Cable, N. B. English, D. D. Ignace, J. A. Eilts, M. J. Mason, J. F. Weltzin, and D. G. Williams (2006), Antecedent moisture and seasonal precipitation influence the response of canopy-scale carbon and water exchange to rainfall pulses in a semi-arid grassland, *New Phytol.*, *170*, 849–860, doi:10.1111/j.1469-8137.2006.01732.x.

Prince, S. D., and S. N. Goward (1995), Global primary production: A remote sensing approach, *J. Biogeogr.*, *22*, 815–835, doi:10.2307/2845983.

Renard, K. G., L. J. Lane, J. R. Simanton, W. E. Emmerich, J. J. Stone, M. A. Weltz, D. C. Goodrich, and D. S. Yakowitz (1993), Agricultural impacts in an arid environment: Walnut Gulch studies, *Hydrol. Sci. Technol.*, *9*, 145–190.

Savage, K. E., and E. A. Davidson (2003), A comparison of manual and automated systems for soil CO_2 flux measurements: trade-offs between spatial and temporal resolution, *J. Exp. Bot.*, *54*(384), 891–899, doi:10.1093/jxb/erg121.

Schott, J. R., J. S. Barsi, B. L. Nordgren, N. G. Raqueno, and D. de Alwis (2001), Calibration of Landsat thermal data and application to water resource studies, *Remote Sens. Environ.*, *78*, 108–117, doi:10.1016/S0034-4257(01)00253-X.

Scott, R. L., T. E. Huxman, W. L. Cable, and W. E. Emmerich (2006), Partitioning of evapotranspiration and its relation to carbon dioxide exchange in a Chihuahuan Desert shrubland, *Hydrol. Processes*, *20*, 3227–3243, doi:10.1002/hyp.6329.

Seber, G. A. F., and C. J. Wild (2003), *Nonlinear Regression*, Wiley-Intersci., Hoboken, N. J.

Shuahua, Q., Z. YuanPei, N. Zhang, W. ChangYao, and Z. Lin (2005), Application of water deficit index in drought monitoring in China with remote sensing, *Turang Xuebao*, *42*(3), 367–372.

Skirvin, S., M. Kidwell, S. Biedenbender, D. King, S. Moran, and C. Holifield Collins (2008), Long-term vegetation transect database, WGEW, Arizona, USA, *Water Resour. Res.*, doi:10.1029/2006WR005724, in press.

Svejcar, T., H. Mayeux, and R. Angell (1997), The rangeland carbon dioxide flux project, *Rangelands*, *19*(5), 16–18.

Valentini, R., et al. (2000), Respiration as the main determinant of carbon balance in European forests, *Nature*, *404*, 861–865, doi:10.1038/35009084.

Vidal, A., and C. Devaux-Ros (1995), Evaluating forest fire hazard with a Landsat TM derived water stress index, *Agric. For. Meteorol.*, *77*, 207–224, doi:10.1016/0168-1923(95)02262-V.

Wilson, K. B., and D. D. Baldocchi (2001), Comparing independent estimates of carbon dioxide exchange over 5 years at a deciduous forest in the southeastern United States, *J. Geophys. Res.*, *106*(D24), 34,167–34,178, doi:10.1029/2001JD000624.

Wohlfahrt, G., C. Anfang, M. Bahn, A. Haslwanter, C. Newesely, M. Schmitt, M. Drösler, J. Pfadenhauer, and A. Cernusca (2005), Quantifying nighttime ecosystem respiration of a meadow using eddy covariance, chambers and modeling, *Agric. For. Meteorol.*, *128*, 141–162, doi:10.1016/j.agrformet.2004.11.003.

Wylie, B. K., D. A. Johnson, E. Laca, N. Z. Saliendra, T. G. Gilmanov, B. C. Reed, L. L. Tieszen, and B. B. Worstell (2003), Calibration of remotely sensed, coarse resolution NDVI to CO_2 fluxes in a sagebrush-steppe ecosystem, *Remote Sens. Environ.*, *85*, 243–255, doi:10.1016/S0034-4257(03)00004-X.

Wylie, B. K., T. G. Gilmanov, D. A. Johnson, N. Z. Saliendra, K. Akshalov, L. L. Tieszen, and B. C. Reed (2004), Intra-seasonal mapping of CO_2 flux in rangelands of northern Kazakhstan at one-kilometer resolution, *Environ. Manage.*, *33*(S1), S482–S491, doi:10.1007/s00267-003-9156-8.

Xiao, X., D. Hollinger, J. Aber, M. Goltz, E. A. Davidson, Q. Zhang, and B. Moore III (2004), Satellite-based modeling of gross primary production in an evergreen needleleaf forest, *Remote Sens. Environ.*, *89*, 519–534, doi:10.1016/j.rse.2003.11.008.

R. B. Bryant, W. E. Emmerich, M. Hernandez, C. D. Holifield Collins, M. S. Moran, R. L. Scott, and C. L. Verdugo, Southwest Watershed Research Center, Agricultural Research Service, U.S. Department of Agriculture, Tucson, AZ 85719, USA.

D. M. King, School of Natural Resources, University of Arizona, Tucson, AZ 85721, USA.